Ecological Informatics 81 (2024) 102624

Contents lists available at ScienceDirect

Ecological Informatics

journal homepage: www.elsevier.com/locate/ecolinf

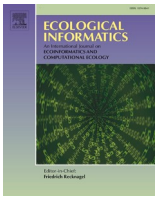

Aquatic vegetation mapping with UAS-cameras considering phenotypes

Loránd Szabó [a], László Bertalan [a,*], Gergely Szabó [a], István Grigorszky [b], Imre Somlyai [b], György Dévai [b], Sándor Alex Nagy [b], Imre J. Holb [c,d], Szilárd Szabó [a]

[a] Department of Physical Geography and Geoinformation Systems, University of Debrecen, H-4032 Egyetem tér 1, Debrecen, Hungary
[b] Department of Hydrobiology, University of Debrecen, H-4032 Egyetem tér 1, Debrecen, Hungary
[c] Institute of Horticulture, University of Debrecen, H-4032 Böszörményi út 138, Debrecen, Hungary
[d] Plant Protection Institute, Centre for Agricultural Research, Eötvös Loránd Research Network (ELKH), Herman Ottó út 15, 1022 Budapest, Hungary

ARTICLE INFO

Keywords:
Image classification
Spectral index
Texture index
DSM
Data fusion
UAS
Recursive feature elimination
Aquatic vegetation

ABSTRACT

Aquatic vegetation species at the genus level in an oxbow lake were identified in Hungary based on a multispectral Uncrewed Aerial System (UAS) survey within an elongated oxbow lake area of the Tisza River under continental climate. Seven and 13 classes were discriminated using three different classification methods (Support Vector Machine [SVM], Random Forest [RF], and Multivariate Adaptive Regression Splines [MARS]) using different input data in ten combinations: original spectral bands, spectral indices, Digital Surface Model (DSM), and Haralick texture indices. We achieved a high (97.1%) overall accuracies (OAs) by applying the SVM classifier, but the RF performed only <1% worse, as it was represented in the first places of the classification rank before the MARS. The highest classification accuracies (>84% OA) were obtained using the most important variables derived by the Recursive Feature Elimination (RFE) method. The best classification required DSM as an input variable. The poorest classification performance belonged to the model that used only texture indices or spectral indices. On the class level, *Stratiotes aloides* exhibit the lowest degree of separability compared to the other classes. Accordingly, we recommend using supplementary input data for the classifications besides the original spectral bands, for example, DSM, spectral, and texture indices, as these variables significantly improve the classification accuracies in the proper combinations of the input variables.

1. Introduction

The growing importance of the multipurpose use of aquatic and wetland habitats has led to increased attention to the significance of ecosystem services (Biggs et al., 2017; Mitsch et al., 2015). Without understanding these services, it is difficult to achieve the sustainable use of water bodies that meet economic, health, recreational, and conservation requirements (Das et al., 2022; Deng et al., 2016; Sannigrahi et al., 2020). The usability of water bodies depends heavily on the knowledge of their natural state and the extent of changes and processes occurring within them. Habitat conditions are well characterized by the organisms and vegetation present in the area (Akwuma and Ezra, 2023; Dömötörfy et al., 2003; Petrů et al., 2016). The presence and diversity of organisms and vegetation in an area provide valuable information that can be challenging and time-consuming to obtain. As the hydrology and ecology of an area change, some organisms may be displaced from their original habitat, whereas others may colonize new areas in large numbers, even invasively, in a relatively short period (Peterson et al., 2008; Tyler et al., 2018).

Improving the classification accuracy is a permanent task for modelers, and this is especially true in remote sensing. To achieve higher precision in classifying land cover, a comprehensive approach is necessary for the integration of diverse data sources and the adoption of sophisticated algorithmic techniques. Better classification performance can be achieved using better input data, that is, better spatial resolution (Szabó et al., 2019, 2020; Tan et al., 2020). Higher resolution and deeper details of the objects enable better identification rates with better outlines, for example, buildings cannot even appear in a MODIS image due to coarse resolution, while Landsat 4–9 or Sentinel-2 indicate the larger ones; for a building footprint, one needs PlanetScope, SkySat, or WorldView imagery (Ganjirad and Bagheri, 2024; Matiza et al., 2024; Wang et al., 2018; Xing et al., 2023). Increasing the number of spectral bands has the potential to improve the classification performance. In addition to the visible spectral range, if we include the infrared

* Corresponding author.
E-mail address: bertalan@science.unideb.hu (L. Bertalan).

https://doi.org/10.1016/j.ecoinf.2024.102624
Received 4 December 2023; Received in revised form 29 April 2024; Accepted 29 April 2024
Available online 6 May 2024

spectrum, the identification of vegetation and the water surface is highly efficient (Kellaris et al., 2019). Complementing spectral data with ancillary information, such as elevation data and spectral and texture indices, further enriches the classification process. These ancillary datasets provide supplementary information that enhances the accuracy of classifying environmental features. Incorporating spatial data, such as Digital Surface Models (DSMs), serves as a foundational step towards a more holistic understanding of wetland landscapes. DSMs enable the comprehensive visualization of topographic variability and structural features within the investigated areas. Novel methods, that is, classification algorithms, especially combined with hyperparameter tuning that optimizes performance, can ensure robust classifiers without assumptions or requirements on large training datasets (Recknagel and Staiano, 2019). Training data augmentation, which extends the existing training data, enhances the generalization capabilities (Likó et al., 2023). Post-classification, generally segmentation, and filtering generally provide better maps with a lower rate of salt-and-pepper errors (Ahmed et al., 2017). We can also deal with the characteristics of the geometry of the training data, excluding outliers, refining the training samples, or changing the proportion of the training and test data. These strategies collectively improve classification accuracy, enabling better modelling of the environment.

To attain a deeper level of understanding, it is important to implement a more refined categorization of land cover classes. The decision to categorize vegetation genotypes into phenophases or subcategories based on visual appearance has the potential to improve the classification performance. In certain contexts, such as consistent environments, such as forests, phenophase-based classification of multi-temporal time series can yield reliable results. This approach leverages the consistency of vegetation appearance over time and can potentially enhance the accuracy of the classification outcomes. However, it is important to confirm that relying only on the visual characteristics captured in a single image might introduce uncertainties in a more diverse and variable environment. In wetland areas, the complexity of environmental factors, such as high diversity, mixed vegetation, varying species content by season or year, and the potential for variations in appearance due to changing conditions, even the movement of floating vegetation, could affect the accuracy of such classifications, where multi-temporal image processing cannot be applied.

Several studies have successfully applied these methods. Tree species were successfully classified by applying multi-temporal imagery and a Random Forest (RF) classifier combined with variable selection (Jing et al., 2009; Persson et al., 2018). Maize genotypes can also be classified with a 30% increment in accuracy by applying multi-temporal images instead of using only single images (Walter, 2020). These studies prove that in consistent environments, for example, croplands, forest species, or genus-level classification, different phenophases can be identified as well. Although wetland areas are not as consistent as these environments, studies have also observed them. Using Uncrewed Aerial Systems (UASs), we are able to perform long-term wetland monitoring, including inundation, water turbidity, water depth, and aquatic plant cover (Alvarez-Vanhard et al., 2020; Deng et al., 2022; Díaz-Delgado et al., 2019; Eltner et al., 2021; Manfreda et al., 2018). The development of imaging and analysis technologies using uncrewed aerial vehicles has facilitated the detection and monitoring of various problems, which is crucial for their effective use (Kyristsis et al., 2016; Marchessaux et al., 2023). Several studies have explored the conservation implications of UAS-based imaging using different techniques (Baena et al., 2018; Müllerová et al., 2017; Tulldahl and Wikström, 2012; Woellner and Wagner, 2019). In many cases, the emergence of an invasive taxon can lead to rapid changes in vegetation composition and cover in an area (Davis, 2010). Therefore, monitoring invasive taxa is critical to prevent their spread. These investigations are essential, as changes in biotic assemblages, such as aquatic plants, often indicate new or increasing anthropogenic impacts on the site. Therefore, the prediction of habitat processes is highly reliant on these observations (Babko et al., 2012; Bolpagni et al., 2020; Del Pozo et al., 2011; Elo et al., 2018; Wilk-Woźniak et al., 2019).

Enhancing the accuracy and usability of UAS methods can significantly aid in determining the necessity and timing of compensatory intervention. The resulting models can serve as efficient inputs for wetland dynamics and habitat diversity assessments. Using different machine learning algorithms involving vegetation indices, texture images, and height parameters as well as classifications, we have the potential to detect species such as *Phragmites australis* in a wetland area (Abeysinghe et al., 2019). The studies in question have primarily concentrated on the categorization of different land cover classes without any further subdivision into subclasses, regardless of whether they are based on specific species or varying stages of phenophase. Therefore, the implementation of hierarchical classification methodologies that employ multiple levels can be useful in distinguishing between broader and more specific categories of land cover. While certain studies have adopted a hierarchical approach to classify genetic subclasses (Ahmed et al., 2017; Jiao et al., 2019; S. Garcia et al., 2019; Walker et al., 2010; Xing et al., 2023), none have incorporated diversification with respect to varying phenophases and visual disparities. Furthermore, the impact of different input datasets and classifiers on the enhancement of classification methodology has not been explored in these studies.

Phenophase variations present in an area at the same time can be effectively emphasized through the introduction of subcategories (Ahmed et al., 2017; Jiao et al., 2019). More classes of classification offer a sophisticated framework for investigating the composition and dynamics of aquatic systems. A broad exploration of the complexities of genera and phenophases can improve our understanding of the ecological factors affecting wetland ecosystems and their adaptive responses to environmental processes. The integration of spatial, spectral, and auxiliary data, coupled with the refinement of subclasses, may enhance the precision and accuracy of the classification results. This comprehensive strategy can empower the identification of not only broad-level classes, but also fine-grained differences in habitats (Burai et al., 2015; Kok et al., 2021; Melgani and Bruzzone, 2004). Although vegetation mapping has answered several questions regarding the possibilities of using remote sensing techniques, species identification still poses a challenge. UASs ensure detailed maps with high spatial resolution; however, owing to different sensors, the outputs have varying issues with the recorded values in the pixels. Accordingly, comprehensive analyses regarding the capabilities and different approaches to reducing misclassifications are still the focus of mapping.

The aim of this study was to reveal: i) is the classification more effective by dividing the land cover classes into subclasses (genus types into phenophases); ii) what is the highest overall accuracy (OA) that can be reached during the classifications and which land cover class reaches the highest class level accuracy; iii) which phenophase can be separated with the highest confidence; and iv) what is the optimal input data combination during the classifications for mapping aquatic vegetation?

2. Materials and methods

2.1. Study area

The study area is located in northeastern Hungary, between Rakamaz and Tiszanagyfalu (Fig. 1). The Nagy-morotva is a large elongated oxbow lake of the Tisza River near Rakamaz, with a total length of 4 km and width varying between 100 and 300 m. Of the 1.11 km^2 large study area, the oxbow lake itself covered approx. 0.63 km^2 area. The habitat includes open water, trees, herbaceous plants (*Phragmites australis, Typha angustifolia*), and aquatic plants (*Trapa natans, Nymphaea alba, Stratiotes aloides*) (Burai et al., 2010).

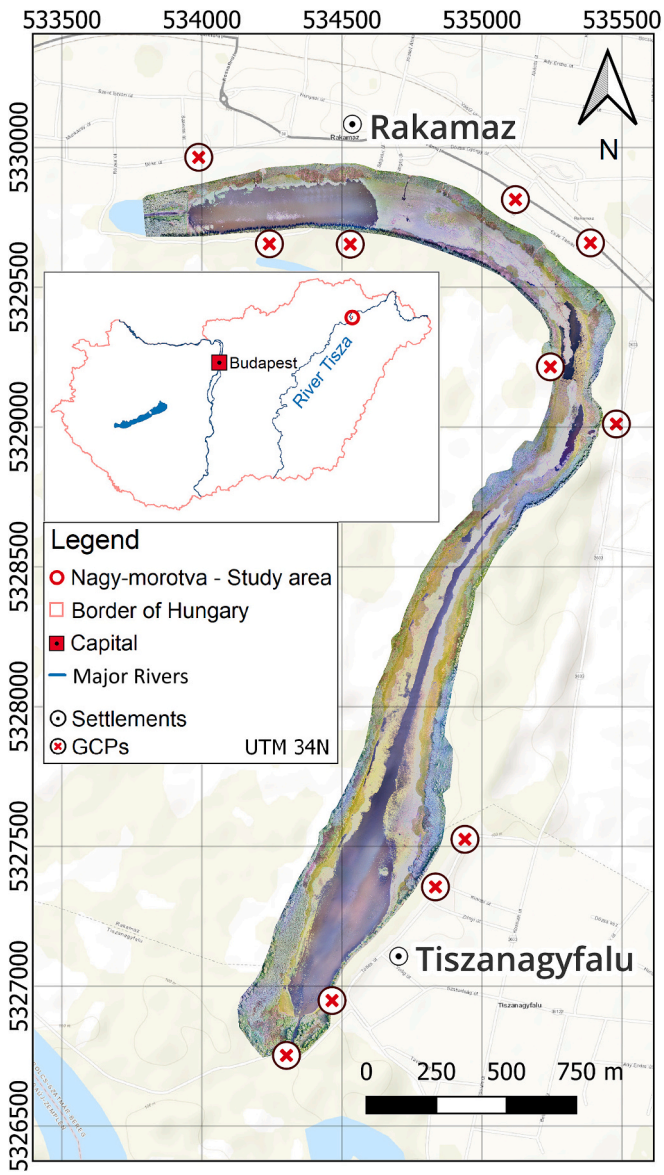

Fig. 1. The study area at the oxbow lake (Nagy-morotva) of Tisza River between Rakamaz and Tiszanagyfalu, Hungary (overlay: true color orthomosaic from the Uncrewed Aerial System survey; Projection: Universal Transversal Mercator (UTM), Zone 34 North).

2.2. UAS survey and data processing

We conducted an aerial survey using a DJI Matrice M200 quadcopter UAS with a Parrot Sequoia multispectral camera on board. The sensor has four monochrome spectral bands (green [530–570 nm], red [640–680 nm], red edge [730–740 nm], and near-infrared [770–810 nm]) and an additional red-green-blue (RGB) lens. An external sunshine sensor module was also mounted on top of the drone to determine the ambient light and sun angle for each band, with the purpose of correcting lighting changes over the study area. The aerial survey was conducted on 11th July, 2019. Image acquisition was performed using the DJI Pilot application. The images were captured 120 m above the ground level (a.g.l.). We applied an 80% overlap for both the frontlap and sidelap. The speed of flight at 4 m per second was chosen to satisfy the criteria for the imaging characteristics of the multispectral lenses. Although it is possible to conduct flights with a faster speed for RGB imaging, it could result in distortion and blurriness for the raw multispectral images. We have indicated this context in the manuscript. Accurate exterior orientation of the structure-from-motion (SfM) processing was ensured by placing 11 Ground Control Points (GCPs) evenly distributed over the study area. The GCP coordinates were then surveyed using the Stonex S9 RTK GNSS system with an accuracy of ±4 cm. Image processing was performed in Pix4D Mapper v4.33 (Pix4D SA, n. d.). The mean Root Mean Square Error (RMSE) of the photogrammetric reconstruction within the RGB and multispectral imagery were found to be 0.06 and 0.14 m respectively. Final RGB and multispectral orthomosaics were produced with ground sampling distances (GSD) of 4 cm and 16 cm, respectively. As described above, Parrot Sequoia camera features two types of lenses, namely an optical RGB lens and four multispectral lenses. These lenses are used in conjunction for aerial image acquisition, and while they share the same altitude above ground level, they differ in focal length, field of view, and sensor size. Consequently, the GSD of the orthophotographs produced by these lenses varies. The absolute reflectance values were derived from the raw multispectral bands during the radiometric calibration in the Pix4D Mapper using the Airinov calibration target supplied with the Sequoia camera (Deng et al., 2018; Olsson et al., 2021). A single set of calibration images was captured, showing the target panel at the beginning of multispectral flights. A Digital Surface Model (DSM) with a spatial resolution of 16 cm was generated through SfM processing of RGB imagery. The processing steps are illustrated in Fig. 2. Three spectral indices were calculated from the multispectral bands: the Normalized Difference Vegetation Index (NDVI; Eq. 1), Normalized Difference RedEdge Index (NDRE, Eq. 2), and visible NDVI (vNDVI, Eq. 3). The NDVI is a vegetation index that can estimate the amount of biomass in an area. The NDVI quantifies the greenness of pixels (Cao et al., 2018; Li et al., 2021; Rouse et al., 1974; Tucker, 1979). NDRE is a unique red-edge index that can detect stress in vegetation; thus, it can measure slight differences in vegetation (Barnes et al., 2000; Eitel et al., 2011). vNDVI is a visible NDVI index that estimates NDVI values from RGB data and provides further information on vegetation by expressing greenness differently way (Costa et al., 2020).

$$NDVI = \frac{NIR - RED}{NIR + RED} \tag{1}$$

$$NDRE = \frac{NIR - RE}{NIR + RE} \tag{2}$$

$$vNDVI = \frac{GREEN - RED}{GREEN + RED} \tag{3}$$

where NIR is the near-infrared band, RE is the red-edge band, RED is the red band, GREEN is the green band.

Texture, that is, the spatial pattern of the objects, can be unique (e.g., homogenous, heterogeneous); thus, they can help discriminate classes when spectral features are similar and simple statistics such as mean or standard deviation do not show differences. Texture indices (or Haralick indices) were calculated based on the gray level co-occurrence matrix (GLCM). The calculation is based on the analysis of two pixels, the reference and neighboring pixels, and a matrix is built based on the kernel size (size of the moving window where co-occurrence values are counted) and offset (distance of reference and neighboring pixels). Finally, the co-occurring intensity pairs of the gray level provide GLCM. Accordingly, images should be converted to 4 or 8-bit because too many pairs would be 0 owing to lack of co-occurrence, which leads to a weak approximation of the pattern (Hall-Beyer, 2017). From several texture indices, the Run percentage performed well, with the highest importance in previous research (Schlosser et al., 2020), thus, we calculated the Run percentage (Eq. 4), using the 8-bit version of the NDVI layer in the Orfeo Toolbox in the QGIS 3.16 environment (Grizonnet et al., 2017; Miyamoto and Jr, 2008) with nine different kernel and offset parameters. NDVI was selected because it preserved band information, represented biomass, and guaranteed visually distinct features for various genus groups. The following parameters were applied: two, three, and five kernel (k) options and one, three, and five offset (o) options in all

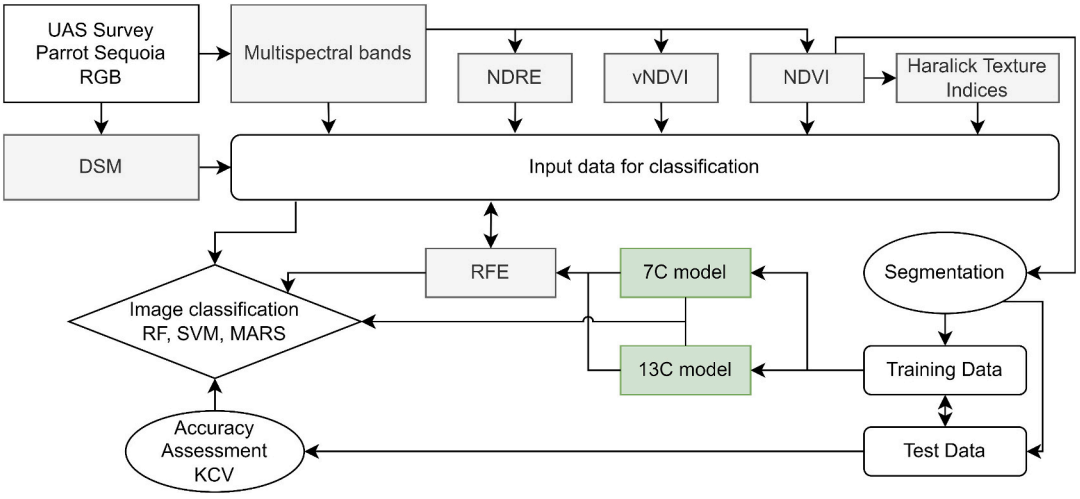

Fig. 2. Processing flowchart of the approach applied in this study (Uncrewed Aerial System [UAS], Red-Green-Blue [RGB], Digital Surface Model [DSM], Normalized Difference Vegetation Index [NDVI], Normalized Difference RedEdge Index [NDRE] and visible NDVI [vNDVI], 7 class [7C], 13 class [13C], Recursive Feature Elimination [RFE], Support Vector Machine [SVM], Random Forest [RF], Multivariate Adaptive Regression Splines [MARS], K-fold Cross Validation [KCV]). (For interpretation of the references to color in this figure legend, the reader is referred to the web version of this article.)

combinations (9).

$$Run\ percentage = \sum_{i=1}^{Ng}\sum_{i=1}^{Nr} p(i,j) \Big/ P \tag{4}$$

where Ng is the number of gray levels in the quantized image, Nr is the number of run lengths, P is the number of points in the image, and p(i,j) is the $(i,j)^{th}$ entry in a normalized gray-tone spatial dependence matrix and in the given run-length matrix.

2.3. Image classification

First, an object-based segmentation was applied with the seeded region growing algorithm using the NDVI layer in SAGA GIS v7.9

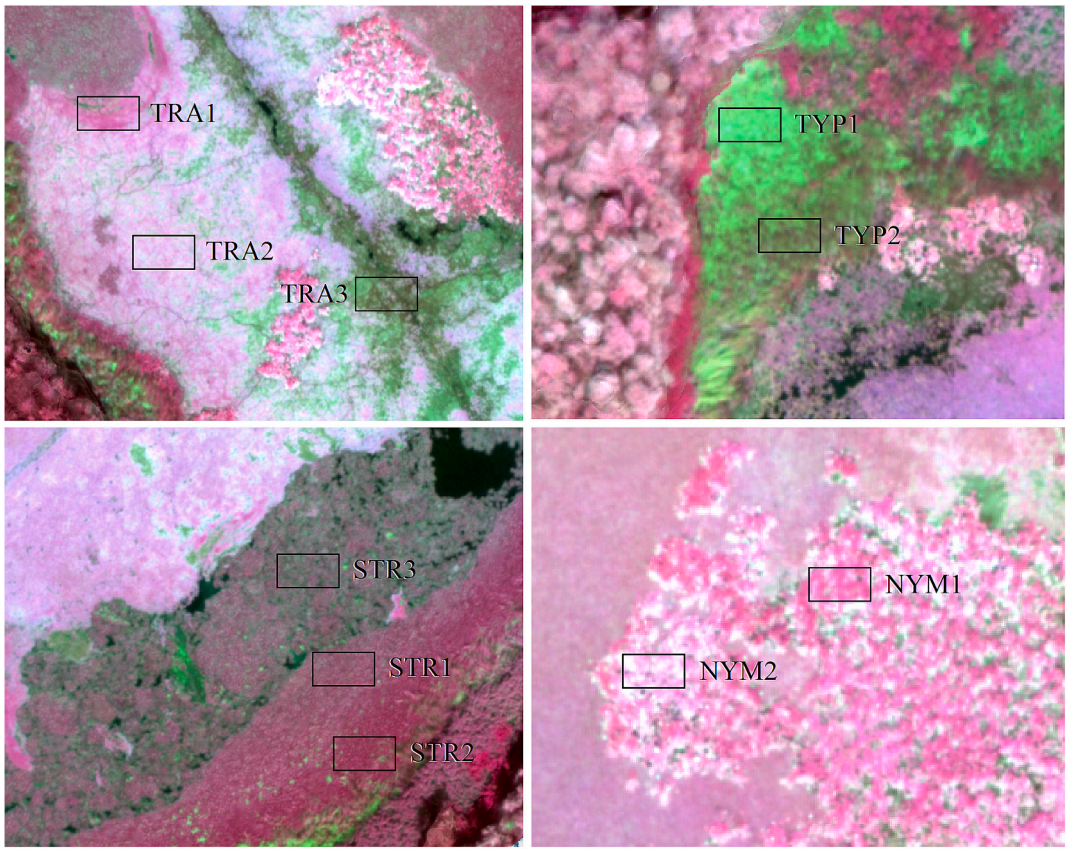

Fig. 3. Appearance of the different phenophases of the divided genus types illustrated on the color-infrared composite of the Parrot Sequoia image (*Trapa natans* [TRA] initial (1), mature (2) and senescence (3) stages; *Stratiotes aloides* [STR] dense floating (1) dense rooted (2) and dispersed (3) stages; mixed *Typha* species [TYP] initial (1) and mature (2) stages; *Nymphaea alba* [NYM] initial (1) and mature (2) stages).

Table 1
Hyperparameters in the grid search.

Algorithm	Hyperparameter ranges
RF	mtry: 1–20 with increments of 1
SVM	gamma: 0.01–0.1 with increments of 0.01 C: 2–16 with increments of 2
MARS	degree: 1–3 nprune: 2 to 100 with increments of 10

(Conrad et al., 2015). The optimal segment size was chosen based on the extent of the patches, without losing any elements of the species pattern. The mean values of the segments were used for classification. Segments are optimal to avoid spatial autocorrelation when using k-fold cross-validation (KCV) in the model-building and/or accuracy assessment phase.

We classified seven land cover categories (7C) over the study area: open water (WAT), mixed *Salix* species (SAL), *Phragmites australis* (PHR), mixed *Typha* species (TYP), *Trapa natans* (TRA), *Nymphaea alba* (NYM) and *Stratiotes aloides* (STR). Next, we split the TRA species into three phenophases, as their appearance varied by age (Fig. 3): (1) initial, (2) mature, and (3) senescence stages; (2) STR species into three phenophases (dense floating [STR1], dense rooted [STR2], and dispersed [STR3] stages; (3) TYP's initial (TYP1) and mature stages (TYP2); and) NYM into two phenophases (initial [NYM1] and mature [NYM2]). Accordingly, we also applied a 13-class (13C) version of the analysis (WAT, PHR, SAL, STR1–2-3, NYM1–2, TYP1–2, and TRA1–2-3). We collected 327 segmentation-based polygon reference sites for classification using field surveys and orthophotos.

Altogether, we had 17 variables (spectral bands: green, red, red edge, NIR; spectral indices – NDVI, vNDVI, NDRE, DSM, and nine variations of the texture index, Run Percentage, with three kernel and three offset options in all combinations). We applied different input datasets using combinations of possible variables (Fig. 2 and Table 2). We also determined the most important variables based on the largest OA with the Recursive Feature Elimination (RFE) method. RFE is a variable selection method that can be combined with machine learning algorithms and we used the RF. RFE removes the variable with the lowest contribution from the input set to achieve the highest overall accuracy stepwise: first, the weakest variable is removed and continues until only one variable (with the highest contribution) remains. We applied the RFE in two steps (Chen et al., 2018; Rasel et al., 2021): (i) first we determined the best-performing texture index, and then (ii) combining all variables (original bands, spectral indices, DSM, and the selected best performing texture index) we determined the most important variables for the 7C and the 13C solutions.

Three classification methods were applied: Support Vector Machine (SVM), a robust machine learning technique that uses hyperplanes (Burai et al., 2015; Kok et al., 2021; Melgani and Bruzzone, 2004) with the radial basis function to handle non-linearity; Random Forest (RF), which uses decision trees for classification (Abriha et al., 2018; Belgiu and Drăguţ, 2016; Breiman, 2000; Phinzi et al., 2020); and Multivariate Adaptive Regression Splines (MARS) as a non-parametric extension of regressions, which is insensitive to nonlinearity (Friedman, 1991; Garosi et al., 2019; Rotigliano et al., 2018). All classification models were run with hyperparameter tuning using the grid search method to determine the best sets of function parameters (Table 1). RF has one important hyperparameter, mtry, which controls the input variables for the decision trees. SVM has two parameters to fine-tune: gamma (how large the influence of the training data is: small values define large distance, large values define small distance in the hyperspace defined by the variables), and C (small values increase, large values decrease misclassifications). In the case of MARS, the two parameters are the degree (maximum degree of interactions between input variables) and nprune (controls the number of basis functions to retain).

We classified all the input dataset combinations (10 variable sets; Table 2) with each classifier (RF, SVM, MARS) and with two sets of classes (7C and 13C); thus, we had 60 models as a result of the classifications. Classifications and hyperparameter tuning were conducted in R 4.2 (R Core Team, 2023) with the caret package (Kuhnaut et al., 2022).

2.4. Accuracy assessment

The reference dataset was split into training and testing sets at a 70:30 ratio, and we applied two types of accuracy assessments. (i) In the model building phase, using the training dataset, we applied 10-fold cross-validation with three repetitions. The training dataset was randomly split into 10 folds; 9 folds were used for model training and 1 for testing, and this procedure ended when all folds were testing data. The whole sequence was repeated using two new random splits (Abriha et al., 2023; Molinaro et al., 2005). This type of accuracy assessment, with hyperparameter tuning, helps to find the best models with the largest overall accuracy (OA), and also reflects the resulting 30 OAs distribution models with minimums, maximums, quartiles, and medians. The smaller the range of possible model outcomes (OAs), the more reliable the prediction. (ii) Based on the testing dataset, we predicted the models and calculated the user's accuracies (UAs) and producer's accuracies (PAs).

2.5. Separability assessment

We applied separability analysis based on the Jeffries-Matusita distance (JM) in the case of both the 7C and 13C models. JM is a separability criterion used to estimate the separability of the spectral features by class. The values range between 0 and 2, where 0 indicates no possible separability, and 2 indicates the maximal separability potential (Bruce et al., 2021; Dabboor et al., 2014; Sen et al., 2019). In our study, we calculated JM from the variables selected by the RFE and assessed the separability of the land cover classes. JM matrix was calculated using R 4.2.3 (R Core Team, 2023) with the varSEL package (Richards, 2013).

Table 2
The different combinations of input datasets used for the classifications (Near Infrared [NIR], Normalized Difference Vegetation Index [NDVI], Normalized Difference RedEdge Index [NDRE] and visible NDVI [vNDVI], Digital Surface Model [DSM], kernel [k] and offset [o] values applied during the Run Percentage calculation).

Code	Description	Input data
a	all type	GREEN, RED, REDEDGE, NIR, NDRE, NDVI, vNDVI, DSM, Run Percentage (k5o1)
b	spectral bands	GREEN, RED, REDEDGE, NIR
si	spectral indices	NDVI, NDRE, vNDVI
t	texture indices	Run Percentage (k2o1, k2o3, k2o5, k3o1, k3o3, k3o5, k5o1, k5o3, k5o5)
bsi	bands and spectral indices	GREEN, RED, REDEDGE, NIR, NDRE, NDVI, vNDVI
rfe	variable selection with Recursive Feature Elimination of the 7 class model	DSM, REDEDGE, NIR, vNDVI, GREEN, NDVI
	variable selection with Recursive Feature Elimination of the 13 class model	REDEDGE, vNDVI, DSM, NIR, NDRE, NDVI
tsi	texture index and spectral indices	Run Percentage (k5o1), NDVI, NDRE, vNDVI
tb	texture index and spectral bands	Run Percentage (k5o1), GREEN, RED, REDEDGE, NIR
db	DSM and spectral bands	DSM, GREEN, RED, REDEDGE, NIR
dsi	DSM and spectral indices	DSM, NDRE, NDVI, vNDVI

JM values were squared to achieve the common JM value range of 0–2 as the varSel used a different function (with the square root of JM).

3. Results

3.1. Jeffries-Matusita separability analysis

The applied JM distance separability analysis indicated that the most separable class was WAT among the land cover classes of the 7C approach (Fig. 4), as it reached the highest values (2.000) for each class. High (>1.93) values were obtained for the NYM and TYP classes. The SAL category had high (>1.99) values in the case of the WAT, TRA, and TYP classes, lower values in the case of the STR (1.944) and NYM (1.972), and the lowest value was obtained between the SAL and PHR (1.772). The PHR and TRA also reached a low values in the STR (1.825 and 1.877).

JM values of the 13C approach showed that the WAT had the highest value (2.000) compared to all other classes (Fig. 5). High values (>1.98) were also observed in the NYM2 and TYP1 classes against all other classes, except between TYP1 and TYP2 (1.714). The worst values were observed among the three STR classes (1.492–1.838). Poor separability values were observed between PHR and SAL (1.843), PHR and STR3 (1.881), and TRA1 and STR1 (1.839) and STR2 (1.877).

3.2. Selection of input variables

Thirty models of the 10 input datasets with three classifiers revealed that the best five medians belonged to the SVM and RF, while the MARS was only ranked 6th (7C) and 10th (13C) (Fig. 6). The best OAs were 96.1% (7C) and 85.4% (13C), and the model performance also depended on the input datasets, while the best accuracy of 7C was obtained with the RFE variable selection dataset. In the case of 13C, it required the use of all variables; nevertheless, the RFE dataset ensured only slightly (1.1%) worse OA. Regarding the minimum OAs, RF (with the RFE dataset) provided 3.8% better results than the SVM (with the RFE dataset; 80.7%) in the case of 7C, and we experienced the same in the case of 13C, but the difference was only 1.9%. The texture index alone was the worst input data, with median OAs of 38.8% and 30.9% (7C and 13C, respectively), followed by 74.0% and 66.6% for spectral indices, respectively. Most models were in the range of 80–90% median OAs for the 7C and 65–80% for the 13C approach.

RFE selected six variables and also determined the variable importance rank for 7C: DSM > RE > NIR > vNDVI > GREEN > NDVI and six variables with slight differences for the 13C approach: RE > vNDVI >DSM > NIR > NDRE > NDVI, but the importance varied. The variables selected by RFE also varied based on the number of classes. The DSM, RE, NIR, vNDVI, and NDVI variables were common to both the 7C and 13C approaches. The 7C model included the GREEN band as an additional variable, whereas the 13C model included NDRE.

3.3. Class level evaluation

The 13C SVM classification, which involved all variables (Table 3), resulted in the highest OA (84.54%). Based on the class level accuracies, 100% UAs were produced by the two NYM categories: WAT, TRA1, TRA3, and TYP1. Among these, 100% PAs were reached by NYM2, WAT, and TRA1. Additionally, TRA2 reached 100% PA. The worst UAs were produced by STR3 (44.44%) and TYP2 (50.00%). The UA of the other classes was higher than 75.00%. The worst PA was produced by STR1 (42.86%), and 60.00% PAs were produced by the two types of TYP, and 66.67% by TRA3. The proportion of other PAs was higher than 75.00%. Significant misclassification was observed for the three STR classes. Both the UA and PA values were lower in the SAL and TYP2 categories.

Visualizing the UA and PA values (Fig. 7) of the 7C SVM RFE classification and 13C SVM classification involving all variables, we observed that the 7C approach reached higher values in the case of both UA and PA. The worst value belonged to the PA of the TYP (0.82). Better PAs were reached by the PHR (0.89) and SAL (0.91) classes, while the other classes reached the maximum PAs (1.00). On the UAs side, STR (0.87) and SAL (0.91) classes had values that were different from 1.00. The 13C approach resulted in a more diverse outcome, as the UA values varied between 0.44 and 1.00 and the PA values from 0.43 to 1.00. WAT had the highest class-level UA and PA values (0.99), while SAL and PHR were between 0.78 and 0.91. The worst values belonged to the STR subclasses STR1 PA (0.43) and STR3 UA (0.44). The other STR values varied between 0.70 and 0.88. Among the classes, both NYM values were > 0.93. TRA1 also had high (>0.97) UA and PA values, but TRA2 had 0.88 UA next to 1.00 PA and TRA3 had 0.67 PA next to 1.00 UA. In the case of TYP, both categories' PA reached 0.60, while TYP1's UA reached 1.00, and TYP2‘s was only 0.50.

4. Discussion

The significance of remotely sensing plant communities in aquatic environments has been highlighted previously. This method offers a consistent and detailed perspective not only of species composition and its variations over time and space, but also of the relationships between material flow, succession, and water quality (Fu and Zhang, 2024; Ribeiro-Souza et al., 2022).

During our work, we discovered several challenges in identifying plant populations using remote sensing in the field. Moritake et al. (2024) also faced challenging problems during their studies classifying vegetation by human observers versus deep learning classifiers, in our results we also highlight the importance of involving machine learning techniques to gain better accuracy. While it is not difficult to survey and assess populations in deeper oligotrophic lakes in cooler climates, where the species and phenology are predominantly monospecific, the situation is different in shallow and eutrophic water bodies. In these areas, the simultaneous presence of several phenophases and numerous other plant species can result in large variations in plant populations, even within a small area. In their studies Granados et al. (2013) also identified different phenological stages of plant communities, however they

SAL	STR	PHR	NYM	WAT	TRA	TYP	
	1.9437	1.7721	1.9724	2.0000	1.9966	1.9968	SAL
		1.8255	1.9656	2.0000	1.8768	1.9571	STR
			1.9975	2.0000	1.9939	1.9848	PHR
				2.0000	1.9342	2.0000	NYM
					2.0000	2.0000	WAT
						1.9893	TRA
							TYP

Fig. 4. Separability analysis based on Jeffries-Matusita distance of the 7 class model's classes (green values are above 1.9 threshold value, mean better separability capabilities; open water [WAT], mixed *Salix* species [SAL], *Phragmites australis* [PHR], mixed *Typha* species [TYP], *Trapa natans* [TRA], *Nymphaea alba* [NYM] and *Stratiotes aloides* [STR]). (For interpretation of the references to color in this figure legend, the reader is referred to the web version of this article.)

NYM1	NYM2	PHR	SAL	STR1	STR2	STR3	TRA1	TRA2	TRA3	TYP1	TYP2	WAT	
	1.9716	1.9996	1.9764	1.9952	1.9637	1.9980	1.9949	1.9890	1.9999	2.0000	1.9999	2.0000	NYM1
		1.9999	2.0000	2.0000	2.0000	1.9999	2.0000	1.9876	1.9993	2.0000	2.0000	2.0000	NYM2
			1.8429	1.9638	1.9685	1.8806	1.9976	1.9988	1.9996	1.9985	1.9573	2.0000	PHR
				1.9831	1.9020	1.9896	1.9932	1.9997	2.0000	1.9999	1.9767	2.0000	SAL
					1.4923	1.5282	1.8385	1.9989	1.9988	2.0000	1.9829	2.0000	STR1
						1.8376	1.8769	1.9989	1.9991	2.0000	1.9097	2.0000	STR2
							1.9552	1.9930	1.9773	1.9993	1.9082	2.0000	STR3
								1.9668	1.9992	2.0000	1.9966	2.0000	TRA1
									1.9979	2.0000	2.0000	2.0000	TRA2
										1.9787	1.9962	2.0000	TRA3
											1.7139	2.0000	TYP1
												2.0000	TYP2
													WAT

Fig. 5. Separability analysis based on Jeffries-Matusita distance of the 13 class model's classes (green values are above 1.9 threshold value, mean better separability capabilities; open water [WAT], mixed *Salix* species [SAL], *Phragmites australis* [PHR], *Trapa natans* [TRA] initial [1], mature [2], senescence [3], *Stratiotes aloides* [STR] dense floating [1], dense rooted [2] dispersed [3] stages; mixed *Typha* species [TYP], initial [1] mature [2], and *Nymphaea alba* [NYM] initial [1] and mature [2]). (For interpretation of the references to color in this figure legend, the reader is referred to the web version of this article.)

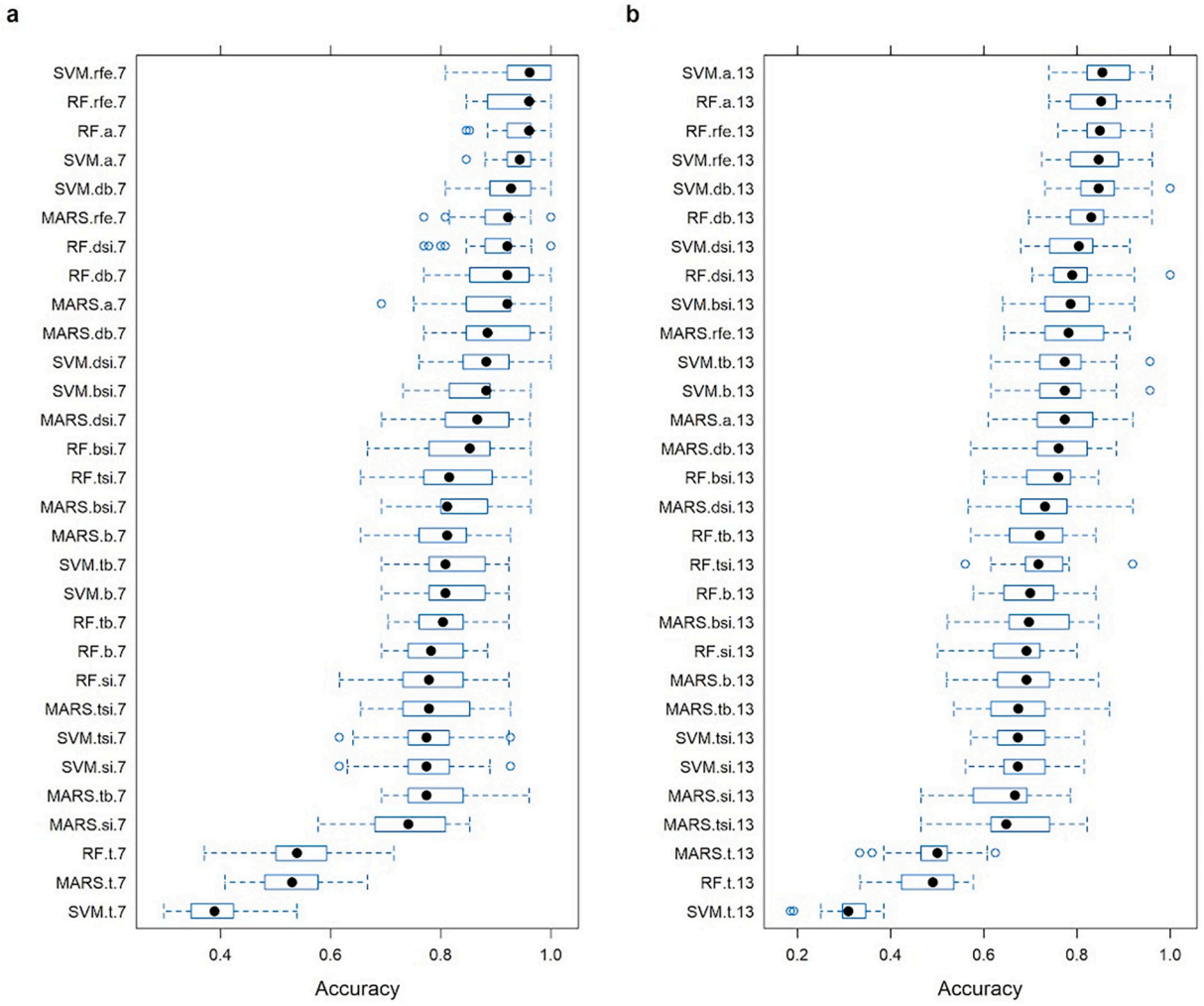

Fig. 6. Distribution of Overall Accuracies of the 30 models of the k-fold cross-validation by 7 (a) and 13 (b) classes (Classifiers: Support Vector Machine [SVM], Random Forest [RF], Multivariate Adaptive Regression Splines [MARS]; input datasets: "a" all input datasets, "b" spectral bands, "si" spectral indices, "t" texture indices, "bsi" bands and spectral indices, "rfe" combined method, "tsi" texture index and spectral indices, "tb" texture index and spectral bands, "db" DSM and spectral bands, "dsi" DSM and spectral indices; •: median, o: outlier, box: lower quartile and upper quartile, whiskers: 1.5 × interquartile range).

applied time series of images, in our study we performed the classification based on a single image, in this case some phenophases were classified with high accuracies (100% UA: NYM1, NYM2, TRA1, TRA3, TYP1; 100% PA: NYM2, TRA1, TRA2), but the 7C model reached higher OAs. Additionally, it can be challenging to distinguish between species belonging to the same genus, such as two representatives of the genus

Table 3
Confusion matrix of the 13C SVM classification involving all variables.

	SAL	STR1	STR2	STR3	PHR	NYM1	NYM2	WAT	TRA1	TRA2	TRA3	TYP1	TYP2	Total %	UA %
SAL	10.31	0.00	0.00	0.00	2.06	0.00	0.00	0.00	0.00	0.00	0.00	0.00	0.00	12.37	83.33
STR1	0.00	3.09	0.00	1.03	0.00	0.00	0.00	0.00	0.00	0.00	0.00	0.00	0.00	4.12	75.00
STR2	1.03	1.03	7.22	0.00	0.00	0.00	0.00	0.00	0.00	0.00	0.00	0.00	0.00	9.28	77.78
STR3	0.00	3.09	1.03	4.12	0.00	0.00	0.00	0.00	0.00	0.00	0.00	0.00	1.03	9.28	44.44
PHR	0.00	0.00	0.00	0.00	7.22	0.00	0.00	0.00	0.00	0.00	0.00	0.00	1.03	8.25	87.50
NYM1	0.00	0.00	0.00	0.00	0.00	13.40	0.00	0.00	0.00	0.00	0.00	0.00	0.00	13.40	100.00
NYM2	0.00	0.00	0.00	0.00	0.00	0.00	1.03	0.00	0.00	0.00	0.00	0.00	0.00	1.03	100.00
WAT	0.00	0.00	0.00	0.00	0.00	0.00	0.00	18.56	0.00	0.00	0.00	0.00	0.00	18.56	100.00
TRA1	0.00	0.00	0.00	0.00	0.00	0.00	0.00	0.00	4.12	0.00	0.00	0.00	0.00	4.12	100.00
TRA2	0.00	0.00	0.00	0.00	0.00	1.03	0.00	0.00	0.00	7.22	0.00	0.00	0.00	8.25	87.50
TRA3	0.00	0.00	0.00	0.00	0.00	0.00	0.00	0.00	0.00	0.00	2.06	0.00	0.00	2.06	100.00
TYP1	0.00	0.00	0.00	0.00	0.00	0.00	0.00	0.00	0.00	0.00	0.00	3.09	0.00	3.09	100.00
TYP2	0.00	0.00	0.00	0.00	0.00	0.00	0.00	0.00	0.00	0.00	1.03	2.06	3.09	6.19	50.00
Total %	11.34	7.22	8.25	5.15	9.28	14.43	1.03	18.56	4.12	7.22	3.09	5.15	5.15	100.00	
PA %	90.91	42.86	87.50	80.00	77.78	92.86	100.00	100.00	100.00	100.00	66.67	60.00	60.00		84.54

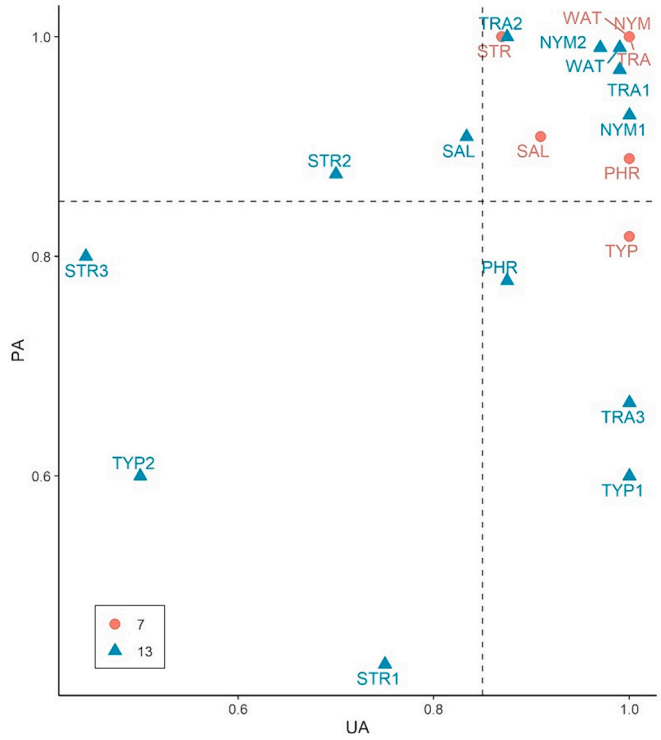

Fig. 7. User's Accuracy (UA) and Producer's Accuracy (PA) values of the 7 class model classification with Support Vector Machine (SVM) classifier involving the input data of the Recursive Feature Elimination method and the 13 class model classification with SVM classifier involving all variables (open water [WAT], mixed *Salix* species [SAL], *Phragmites australis* [PHR], *Trapa natans* [TRA] initial [1], mature [2], senescence [3], *Stratiotes aloides* [STR] dense floating [1], dense rooted [2] dispersed [3] stages; mixed *Typha* species [TYP], initial [1] mature [2], and *Nymphaea alba* [NYM] initial [1] and mature [2]; dashed black line represents 85% accuracy benchmark).

Typha in the Nagy-morotva (*T. angustifolia and T. latifolia*), which are similar and often occur in mixed populations. Therefore, it is appropriate to categorize them at the genus level. However, the coexistence of different phenophases and other plant species mixed in their populations make it difficult for a single taxon, especially in old and shallow eutrophic lakes with a very rich propagule pool. This is true of water caltrop (*Trapa natans*) in the Nagy-morotva, which is protected in Hungary, but has dense populations in many areas, such as the Kisköre reservoir and large pools with vast water surfaces. They are either scattered along the shore towards the open water or gathered in large patches in the bed, with new individuals constantly appearing at the edges towards the open water. Consequently, multiple phenophases can coexist simultaneously, ranging from fresh to dying specimens. The coloration of these individuals varies at different ages, with numerous variations from bright green to reddish-brown occurring within a single population, these color shifts can be efficiently captured in time series as Granados et al. (2013) applied in their studies, although in our case we were also able to distinguish these phenophases for creating the training data. The presence of other plant species in the water caltrop stands, such as *Salvinia natans*, *Hydrocharis morsus-ranae*, and *Lemna* species on the water surface, and *Ceratophyllum demersum*, *Lemna trisulca*, and *Utricularia* species, further complicates identification. This can also have a significant effect on the color effect. Additionally, the degree of invasion by other plant species often varies, even between phenophases, being less noticeable in fresh stands and more noticeable in those in decline. The colocane plant *Stratiotes aloides* displays a similar phenomenon. When it is in good health, its stands are dense and have a vibrant green color. However, when it declines, the stands become scarred, dull, and intermixed with other seaweeds, such as water caltrop. The varying color combinations and structural differences present in the different ages and species compositions of the stands significantly affect reflectance and, in turn, the spectral perception of light.

The uncertainty of the detailed resolution analysis was relatively high in the mixed plant populations (Fig. 7). Therefore, it is more appropriate to focus on the main taxon, such as *Trapa natans* or *Stratiotes aloides*, rather than attempting to separate the different species. However, it is important to note that many wetlands have diverse populations at both phenological and species levels, and surveys providing clear information on these mixed populations are necessary for their accurate characterization.

The results showed that the SVM and RF outperformed the MARS classifier. The best median OA (96.1%) was achieved using the 7C RFE dataset. In the case of the 13C model, applying all input variables yielded the best median OA (85.4%), which indicates that classifying only seven classes without subclasses performed better. Ahmed et al. (2017) classified five land cover classes with 95% OA. Differentiating the classes into subclasses resulted in approximately 82% OAs similar to our results, because the subclasses have similar spectral properties even when they are in different phenological stages. Garcia et al. (2019) also observed a decrease in OAs when broad land cover classes were divided into subclasses. Walker et al. (2010) reported the same decrease in OA values in their study. They also found that ancillary data increased OA. According to our study, we agree that dividing classes decreases OA, as the 7C model performed better than the 13C model, and we also highlight the application of ancillary data next to the spectral bands. Jiao et al. (2019) reported that the OAs were reduced during the classification of 21 classes instead of 13 classes using multispectral data, but applying hyperspectral data detailed classes reached a higher OA (97.38%). Furthermore, the authors found that the hierarchical

Table 4
Relative heights of the vegetation of the Rakamazi Nagy-morotva in relation to the water surface based on the Digital Surface Model.

Land cover class	Abbreviation	Mean relative height (m)	Standard Deviation (m)
Phragmites australis	PHR	3.43	1.11
Stratiotes aloides	STR	0.74	0.92
Mixed *Salix* species	SAL	10.60	6.98
Mixed *Typha* species	TYP	1.10	0.89
Nymphaea alba	NYM	0.12	0.28
Trapa natans	TRA	0.08	0.72

classification method outperformed the single SVM and RF classifiers, where SVM produced more accurate OAs than RF. In our study, we consider the RF a more reliable classifier with a smaller variance of accuracy (OA) related to the SVM, with both the 7C and 13C approaches in agreement with the study of Wang et al. (2019), who reached higher OAs by applying RF instead of SVM. Phinzi et al. (2021) also considered RF as the best classifier in their study. Martínez Prentice et al. (2021) also found that RF has the best performance in both their classifications.

Regarding the input variables, the RFE proved its efficacy with the SVM and RF classifications, which helped reduce the chance of overfitting. Nevertheless, the best OAs were obtained with the RFE for the 7C approach, but for the 13C approach, it was only in the second place; however, only 0.8 worse than including all variables. Varga et al. (2021) found that applying all variables was reasonable and ensured the highest OA. For both the 7C and 13C models, the next most accurate variables were DSM + bands, DSM + spectral indices, and bands+spectral indices as inputs. This indicates the importance of involving a DSM for the classification of aquatic vegetation and highlights the importance of the spectral data, including the original bands and spectral indices. Ayushi et al. (2024) considered elevation data the third most important input variable during their model building. Li et al. (2022) also highlighted the application of DSM, but they found texture indices to be efficient in reaching higher OAs, while in our case, texture indices did not ensure better OAs. In our study, less accurate results were obtained by involving only texture indices, followed by spectral indices, texture indices+-bands, and texture indices+spectral indices. We can conclude that using the texture index as a standalone input may not yield efficient classification results. However, as demonstrated by Li et al. (2022), incorporating it in combination with other significant variables can enhance the classification performance.

The variable importance varied among the models. In the case of the 7C model, the DSM variable was the most important, given that a smaller number of classes encompassed different species and the height variation was largely driven by these distinct species. The RE band was an important variable for both models, in agreement with the study of Díaz-Delgado et al. (2019), who also applied Parrot Sequoia images to assess wetland areas and found that the RE and NIR bands were the best discriminating variables, next to the NDRE index. Xing et al. (2023) highlighted the importance of the RE band, followed by the original spectral bands, vegetation, and water indices. They also applied the RF classifier and RFE variable selection using cross-validation, and the highest OA was 92.36% in their study; accordingly, in our study, the RFE contributed the best two OAs in the case of the 7C model and the third and fourth best OAs in the 13C model. Based on these two studies, we can also confirm the importance of RE, NIR, and NDRE variables, as these were also among the most important variables during our classifications. Laliberte et al. (2011) found that NDVI was the most important variable in their study; however, in our research, NDVI was only the sixth most important variable for both the 7C and 13C models. Ahmed et al. (2017) reported the significance of the NIR band and texture indices as the most important variables, which aligns with our findings, where the NIR band was ranked third among the most critical variables in the context of the 7C model. In the case of subclasses, the authors highlighted the use of height data and texture derivatives. In the context of the 13C model, the digital surface model (DSM) surpassed the NIR band in terms of variable importance ranking. Our findings underscore the substantial role of DSM in classifications, as it emerged as the most crucial variable in the 7C model and held the third position in importance within the 13C model. Martínez Prentice et al. (2021) also found that the Digital Elevation Model is one of the most important variables for the classification of coastal wetlands using high-resolution UAS imagery. Abeysinghe et al. (2019) also successfully classified the PHR using additional input data, such as the canopy height model. In our study, relevant enhancement in classification accuracy was achieved through the inclusion of DSM, a non-conventional practice in classification, which can be attributed to the variation in plant height across the different species in the study area. This variation stems from the fact that each aquatic plant grows at distinct heights while floating on the flat surface of water, underlining the importance of utilizing DSM as supplementary input data for classification. While TRA and NYM barely rise, STR increases, but PHR, TYP and SAL also have different heights. This can be determined from a model calculated using UAS imagery. The disparities in height between the TRA and NYM fell within the tolerance limit, making it challenging to discern such small differences using image acquisition from this height. Consequently, DSM did not prove to be a valuable discriminant variable for these specific classes (Table 4). Incorporating spectral data, including original bands and spectral indices, was augmented by the addition of the surface model as a supplementary data source. This enhancement proved instrumental in distinguishing spectrally similar land cover categories.

Upon comparing class-level accuracies, it was evident that within the top-performing 7C and 13C classification models, the UA and PA values exhibited a narrower range in the case of the 7C model. This observation suggests that the 7C model is more reliable with lower variance and, consequently, can effectively distinguish between broader-level classes. In the case of the 13C model, poor precision values (<0.8) were observed for the three STR classes and TYP2, and, on the PA side, in the case of STR1, STR3, TYP1, TYP2, PHR, and TRA3. These results indicate that separating the STR and TYP into subclasses is not reasonable. We also revealed that considerable misclassification occurred in the subclasses of the different species, especially in the case of the STR, as the different phenophases had similar spectral properties. Similarities were found between TRA3 and TYP3; therefore, misclassified TYP was found in the middle of the lake, which is not possible. Accordingly, phenophase-based subclasses did not help to gain a better model. JM separability analysis proved that WAT was the most separable class in both the 7C and 13C models, as it had a unique spectral signature compared to vegetation. Separability issues arose between PHR, SAL, and STR within the framework of the 7C model, signifying that distinct species may exhibit similar spectral characteristics, and even auxiliary data models failed to effectively differentiate between them. Burai et al. (2010) classified seven land cover classes in the same study area and also faced the same classification problems, as the SAL and PHR were misclassified and found low UA and PA values in the STR class. Although the 13C models had smaller OAs than the 7C models, in the case of some subclasses, we also experienced successful separation, for example, TYP1 and NYM2. TRA3 also achieved high separability results, as this subclass had significantly different spectral properties compared to the other two TRA classes. The worst separable subclasses were the STR classes. Despite the evident differences during visual interpretation,

there were relevant misclassifications among the subclasses. Poor separability values occurred between the PHR, SAL, and STR3 classes, as in the case of the 7C model, indicating that the STR3 type of the STR is less separable from the PHR. The separability analysis also highlighted that the two types of TYP cannot be divided efficiently.

5. Conclusion

In this study, we investigated the classification of aquatic plant communities using remote sensing techniques, with a particular focus on the Rakamazi Nagy-morotva. Our results emphasize the inherent challenges in identifying and classifying plant populations in shallow and eutrophic water bodies where multiple species and phenophases coexist within a limited space. Despite these challenges, the application of machine learning techniques, such as SVM and RF, proved invaluable in achieving high classification accuracies.

The examination of JM separability unveiled WAT as the most separable class, showcasing its unique spectral signature in contrast to other vegetation types. However, challenges in separability were observed between certain classes, such as PHR, SAL, and STR, indicating similar spectral characteristics among distinct species.

Our study underscores the significance of input variables in classification accuracy. The RFE method effectively reduced the likelihood of overfitting, particularly in the 7-class model. Furthermore, incorporating DSM data alongside spectral bands and indices significantly enhanced classification performance, highlighting the importance of height variation in distinguishing different plant species.

The results of our classification analysis indicated disparities between the 7-class and 13-class models, with the former exhibiting higher overall accuracy rates. However, the subdivision of subclasses, particularly in the case of STR and TYP, resulted in decreased precision values. This suggests that broader class distinctions may be more reliable for classification purposes.

Our findings have significant implications for ecosystem monitoring and management, as accurate classification of aquatic plant communities is crucial for assessing ecological health and guiding conservation efforts. Nevertheless, further research is necessary to address the remaining challenges, such as improving the separability between closely related species and refining classification algorithms to accommodate diverse plant populations.

In summary, our study offers valuable insights into the classification of aquatic plant communities using remote sensing techniques, highlighting both successes and areas that require further investigation. By utilizing advanced machine learning methods and incorporating multidimensional data sources, we can continue to enhance our understanding of aquatic ecosystems and contribute to their effective management and conservation.

CRediT authorship contribution statement

Loránd Szabó: Writing – review & editing, Writing – original draft, Visualization, Software, Investigation, Conceptualization. **László Bertalan:** Writing – review & editing, Software, Investigation, Conceptualization. **Gergely Szabó:** Writing – review & editing, Investigation. **István Grigorszky:** Writing – review & editing, Validation, Funding acquisition. **Imre Somlyai:** Writing – review & editing, Validation. **György Dévai:** Writing – review & editing, Validation. **Sándor Alex Nagy:** Writing – review & editing. **Imre J. Holb:** Writing – review & editing, Validation. **Szilárd Szabó:** Writing – review & editing, Writing – original draft, Visualization, Software, Investigation, Funding acquisition, Conceptualization.

Declaration of competing interest

The authors declare that they have no known competing financial interests or personal relationships that could have influenced the work reported in this study.

Data availability

Data will be made available on request.

Acknowledgments

The project was supported by the NKFI K138079 and the RRF 2.3.1 21 2022 00008 projects.

During the preparation of this work the author(s) used Paperpal: AI Academic Writing Tool in order to improve the English of the manuscript. After using this tool/service, the authors reviewed and edited the content as needed and take full responsibility for the content of the publication.

References

Abeysinghe, T., Simic Milas, A., Arend, K., Hohman, B., Reil, P., Gregory, A., Vázquez-Ortega, A., 2019. Mapping invasive phragmites australis in the old woman creek estuary using UAV remote sensing and machine learning classifiers. Remote Sens. 11, 1380. https://doi.org/10.3390/rs11111380.

Abriha, D., Kovács, Z., Ninsawat, S., Bertalan, L., Balázs, B., Szabó, S., 2018. Identification of roofing materials with discriminant function analysis and random Forest classifiers on pan-sharpened WorldView-2 imagery – a comparison. Hung. Geogr. Bull. 67, 375–392. https://doi.org/10.15201/hungeobull.67.4.6.

Abriha, D., Srivastava, P.K., Szabó, S., 2023. Smaller is better? Unduly nice accuracy assessments in roof detection using remote sensing data with machine learning and k-fold cross-validation. Heliyon 9. https://doi.org/10.1016/j.heliyon.2023.e14045.

Ahmed, O.S., Shemrock, A., Chabot, D., Dillon, C., Williams, G., Wasson, R., Franklin, S. E., 2017. Hierarchical land cover and vegetation classification using multispectral data acquired from an unmanned aerial vehicle. Int. J. Remote Sens. 38, 2037–2052. https://doi.org/10.1080/01431161.2017.1294781.

Akwuma, O.D., Ezra, A.G., 2023. Macro-vegetation and physicochemical aspects of Tirwum pond in Bauchi local government area of Bauchi State, Nigeria. Bio-Res. 21, 1953–1960. https://doi.org/10.4314/br.v21i2.3.

Alvarez-Vanhard, E., Houet, T., Mony, C., Lecoq, L., Corpetti, T., 2020. Can UAVs fill the gap between in situ surveys and satellites for habitat mapping? Remote Sens. Environ. 243, 111780 https://doi.org/10.1016/j.rse.2020.111780.

Ayushi, K., Babu, K.N., Ayyappan, N., Nair, J.R., Kakkara, A., Reddy, C.S., 2024. A comparative analysis of machine learning techniques for aboveground biomass estimation: a case study of the Western Ghats, India. Ecol. Inform. 80, 102479 https://doi.org/10.1016/j.ecoinf.2024.102479.

Babko, R., Diachenko, T., Zaburko, J., Danko, Y., Kuzmina, T., Szulzyk-Cieplak, J., Zhigacheva, O.I., 2012. Bioecological peculiarities of water chestnut (Trapa natans L., Trapaceae) in the basin of middle Don (Volgograd region). Вестник Волгоградского государственного университета. Серия 11 (1 1), 1–9 (in Russian).

Baena, S., Boyd, D.S., Moat, J., 2018. UAVs in pursuit of plant conservation - real world experiences. Ecol. Inform. 47, 2–9. https://doi.org/10.1016/j.ecoinf.2017.11.001.

Barnes, E., Clarke, T.R., Richards, S.E., Colaizzi, P., Haberland, J., Kostrzewski, M., Waller, P., Choi, C., Riley, E., Thompson, T.L., 2000. Coincident Detection of Crop Water Stress, Nitrogen Status, and Canopy Density Using Ground Based Multispectral Data.

Belgiu, M., Drăguţ, L., 2016. Random forest in remote sensing: a review of applications and future directions. ISPRS J. Photogramm. Remote Sens. 114, 24–31. https://doi.org/10.1016/j.isprsjprs.2016.01.011.

Biggs, J., Von Fumetti, S., Kelly-Quinn, M., 2017. The importance of small waterbodies for biodiversity and ecosystem services: implications for policy makers. Hydrobiologia 793, 3–39. https://doi.org/10.1007/s10750-016-3007-0.

Bolpagni, R., Laini, A., Buldrini, F., Ziccardi, G., Soana, E., Pezzi, G., Chiarucci, A., Lipreri, E., Armiraglio, S., Nascimbene, J., 2020. Habitat morphology and connectivity better predict hydrophyte and wetland plant richness than land-use intensity in overexploited watersheds: evidence from the Po plain (northern Italy). Landsc. Ecol. 35, 1827–1839. https://doi.org/10.1007/s10980-020-01060-2.

Breiman, L., 2000. Randomizing outputs to increase prediction accuracy. Mach. Learn. 40, 229–242. https://doi.org/10.1023/A:1007682208299.

Bruce, R.W., Rajcan, I., Sulik, J., 2021. Classification of soybean pubescence from multispectral aerial imagery. Plant Phenom. 2021 https://doi.org/10.34133/2021/9806201, 2021/9806201.

Burai, P., Lövei, G., Lénárt, C., Nagy, I., Enyedi, E., 2010. Mapping aquatic vegetation of the Rakamaz-Tiszanagyfalui Nagy-morotva using hyperspectral imagery. Landsc. Environ. 4, 1–10.

Burai, P., Deák, B., Valkó, O., Tomor, T., 2015. Classification of herbaceous vegetation using airborne hyperspectral imagery. Remote Sens. 7, 2046–2066. https://doi.org/10.3390/rs70202046.

Cao, R., Chen, Y., Shen, M., Chen, J., Zhou, J., Wang, C., Yang, W., 2018. A simple method to improve the quality of NDVI time-series data by integrating spatiotemporal information with the Savitzky-Golay filter. Remote Sens. Environ. 217, 244–257. https://doi.org/10.1016/j.rse.2018.08.022.

Chen, Q., Meng, Z., Liu, X., Jin, Q., Su, R., 2018. Decision variants for the automatic determination of optimal feature subset in RF-RFE. Genes 9, 301. https://doi.org/10.3390/genes9060301.
Conrad, O., Bechtel, B., Bock, M., Dietrich, H., Fischer, E., Gerlitz, L., Wehberg, J., Wichmann, V., Böhner, J., 2015. System for automated geoscientific analyses (SAGA) v. 2.1.4. Geosci. Model Dev. 8, 1991–2007. https://doi.org/10.5194/gmd-8-1991-2015.
Costa, L., Nunes, L., Ampatzidis, Y., 2020. A new visible band index (vNDVI) for estimating NDVI values on RGB images utilizing genetic algorithms. Comput. Electron. Agric. 172, 105334 https://doi.org/10.1016/j.compag.2020.105334.
Dabboor, M., Howell, S., Shokr, M., Yackel, J., 2014. The Jeffries–Matusita distance for the case of complex Wishart distribution as a separability criterion for fully polarimetric SAR data. Int. J. Remote Sens. 35, 6859–6873. https://doi.org/10.1080/01431161.2014.960614.
Das, M., Das, A., Seikh, S., Pandey, R., 2022. Nexus between indigenous ecological knowledge and ecosystem services: a socio-ecological analysis for sustainable ecosystem management. Environ. Sci. Pollut. Res. 29, 61561–61578. https://doi.org/10.1007/s11356-021-15605-8.
Davis, M.A., 2010. Researching invasive species 50 years after Elton: A cautionary tale. In: Richardson, D.M. (Ed.), Fifty Years of Invasion Ecology. Wiley, pp. 267–276. https://doi.org/10.1002/9781444329988.ch20.
Del Pozo, R., Fernández-Aláez, C., Fernández-Aláez, M., 2011. The relative importance of natural and anthropogenic effects on community composition of aquatic macrophytes in Mediterranean ponds. Mar. Freshw. Res. 62, 101. https://doi.org/10.1071/MF10125.
Deng, X., Li, Z., Gibson, J., 2016. A review on trade-off analysis of ecosystem services for sustainable land-use management. J. Geogr. Sci. 26, 953–968. https://doi.org/10.1007/s11442-016-1309-9.
Deng, T., Fu, B., Liu, M., He, H., Fan, D., Li, L., Huang, L., Gao, E., 2022. Comparison of multi-class and fusion of multiple single-class SegNet model for mapping karst wetland vegetation using UAV images. Sci. Rep. 12, 13270. https://doi.org/10.1038/s41598-022-17620-2.
Deng, L., Mao, Z., Li, X., Hu, Z., Duan, F., Yan, Y., 2018. UAV-based multispectral remote sensing for precision agriculture: A comparison between different cameras. ISPRS Journal of Photogrammetry and Remote Sensing 146, 124–136. https://doi.org/10.1016/j.isprsjprs.2018.09.008.
Díaz-Delgado, R., Cazacu, C., Adamescu, M., 2019. Rapid assessment of ecological integrity for LTER wetland sites by using UAV multispectral mapping. Drones 3, 3. https://doi.org/10.3390/drones3010003.
Dömötörfy, Z., Reeder, D., Pomogyi, P., 2003. Changes in the macro-vegetation of the Kis-Balaton wetlands over the last two centuries: a GIS perspective. Hydrobiologia 506–509, 671–679. https://doi.org/10.1023/B:HYDR.0000008598.56151.5e.
Eitel, J.U.H., Vierling, L.A., Litvak, M.E., Long, D.S., Schulthess, U., Ager, A.A., Krofcheck, D.J., Stoscheck, L., 2011. Broadband, red-edge information from satellites improves early stress detection in a new Mexico conifer woodland. Remote Sens. Environ. 115, 3640–3646. https://doi.org/10.1016/j.rse.2011.09.002.
Elo, M., Alahuhta, J., Kanninen, A., Meissner, K.K., Seppälä, K., Mönkkönen, M., 2018. Environmental characteristics and anthropogenic impact jointly modify aquatic macrophyte species diversity. Front. Plant Sci. 9, 1001. https://doi.org/10.3389/fpls.2018.01001.
Eltner, A., Bertalan, L., Grundmann, J., Perks, M.T., Lotsari, E., 2021. Hydro-morphological mapping of river reaches using videos captured with UAS. Earth Surf. Process. Landf. 46, 2773–2787. https://doi.org/10.1002/esp.5205.
Friedman, J.H., 1991. Multivariate adaptive regression splines. Ann. Stat. 19, 1–67. https://doi.org/10.1214/aos/1176347963.
Fu, T., Zhang, C., 2024. Towards a generic model evaluation metric for non-normally distributed measurements in water quality and ecosystem models. Ecol. Inform. 80, 102470 https://doi.org/10.1016/j.ecoinf.2024.102470.
Ganjirad, M., Bagheri, H., 2024. Google Earth Engine-based mapping of land use and land cover for weather forecast models using Landsat 8 imagery. Ecol. Inform. 80, 102498 https://doi.org/10.1016/j.ecoinf.2024.102498.
Garcia, S., de Vilela, F.N., Rizzo, R., West, P., Gerber, J.S., Engstrom, P.M., Ballester, R., 2019. Assessing land use/cover dynamics and exploring drivers in the Amazon's arc of deforestation through a hierarchical, multi-scale and multi-temporal classification approach. Remote Sens. Appl. Soc. Environ. 15, 100233 https://doi.org/10.1016/j.rsase.2019.05.002.
Garosi, Y., Sheklabadi, M., Conoscenti, C., Pourghasemi, H.R., Van Oost, K., 2019. Assessing the performance of GIS- based machine learning models with different accuracy measures for determining susceptibility to gully erosion. Sci. Total Environ. 664, 1117–1132. https://doi.org/10.1016/j.scitotenv.2019.02.093.
Granados, J.A., Graham, E.A., Bonnet, P., Yuen, E.M., Hamilton, M., 2013. EcoIP: an open source image analysis toolkit to identify different stages of plant phenology for multiple species with pan–tilt–zoom cameras. Ecol. Inform. 15, 58–65. https://doi.org/10.1016/j.ecoinf.2013.03.002.
Grizonnet, M., Michel, J., Poughon, V., Inglada, J., Savinaud, M., Cresson, R., 2017. Orfeo ToolBox: open source processing of remote sensing images. Open Geospatial Data Softw. Stand. 2, 15. https://doi.org/10.1186/s40965-017-0031-6.
Hall-Beyer, M., 2017. GLCM Texture: A Tutorial v. 3.0 75.
Jiao, L., Sun, W., Yang, G., Ren, G., Liu, Y., 2019. A hierarchical classification framework of satellite multispectral/hyperspectral images for mapping coastal wetlands. Remote Sens. 11, 2238. https://doi.org/10.3390/rs11192238.
Jing, X., Wang, JiHua, Huang, W., Liu, L., Wang, JinDi, 2009. Study on Forest vegetation classification based on multitemporal remote sensing images. In: Li, D., Zhao, C. (Eds.), Computer and Computing Technologies in Agriculture II, IFIP Advances in Information and Communication Technology, vol. 1. Springer US, Boston, MA, pp. 115–123. https://doi.org/10.1007/978-1-4419-0209-2_13.
Kellaris, A., Gil, A., Faria, J., Amaral, R., Moreu-Badia, I., Neto, A., Yesson, C., 2019. Using low-cost drones to monitor heterogeneous submerged seaweed habitats: a case study in the Azores. Aquat. Conserv. Mar. Freshwat. Ecosyst. 29, 1909–1922. https://doi.org/10.1002/aqc.3189.
Kok, Z.H., Mohamed Shariff, A.R., Alfatni, M.S.M., Khairunniza-Bejo, S., 2021. Support vector machine in precision agriculture: a review. Comput. Electron. Agric. 191, 106546 https://doi.org/10.1016/j.compag.2021.106546.
Kuhnaut, M., Wing, J., Weston, S., Williams, A., Keefer, C., Engelhardt, A., Cooper, T., Mayer, Z., Kenkel, B., Team, R. Core, Benesty, M., Lescarbeau, R., Ziem, A., Scrucca, L., Tang, Y., Candan, C., Hunt, T., 2022. caret: Classification and Regression Training.
Kyristsis, S., Antonopoulos, A., Chanialakis, T., Stefanakis, E., Linardos, C., Tripolitsiotis, A., Partsinevelos, P., 2016. Towards autonomous modular UAV missions: the detection, geo-location and landing paradigm. Sensors 16, 1844. https://doi.org/10.3390/s16111844.
Laliberte, A.S., Goforth, M.A., Steele, C.M., Rango, A., 2011. Multispectral remote sensing from unmanned aircraft: image processing workflows and applications for rangeland environments. Remote Sens. 3, 2529–2551. https://doi.org/10.3390/rs3112529.
Li, S., Xu, L., Jing, Y., Yin, H., Li, X., Guan, X., 2021. High-quality vegetation index product generation: a review of NDVI time series reconstruction techniques. Int. J. Appl. Earth Obs. Geoinf. 105, 102640 https://doi.org/10.1016/j.jag.2021.102640.
Li, Y., Deng, T., Fu, B., Lao, Z., Yang, W., He, H., Fan, D., He, W., Yao, Y., 2022. Evaluation of decision fusions for classifying karst wetland vegetation using one-class and multi-class CNN models with high-resolution UAV images. Remote Sens. 14, 5869. https://doi.org/10.3390/rs14225869.
Likó, S.B., Holb, I.J., Oláh, V., Burai, P., Szabó, S., 2023. Deep learning-based training data augmentation combined with post-classification improves the classification accuracy for dominant and scattered invasive forest tree species. Remote Sens. Ecol. Conserv. n/a https://doi.org/10.1002/rse2.365.
Manfreda, S., McCabe, M.F., Miller, P.E., Lucas, R., Pajuelo Madrigal, V., Mallinis, G., Ben Dor, E., Helman, D., Estes, L., Ciraolo, G., Müllerová, J., Tauro, F., De Lima, M.I., De Lima, J.L.M.P., Maltese, A., Frances, F., Caylor, K., Kohv, M., Perks, M., Ruiz-Pérez, G., Su, Z., Vico, G., Toth, B., 2018. On the use of unmanned aerial systems for environmental monitoring. Remote Sens. 10, 641. https://doi.org/10.3390/rs10040641.
Marchessaux, G., Bizzarri, S., Marsiglia, N., Ponzè, N., Sarà, G., 2023. The use of an unmanned aerial vehicle to investigate habitat use and behavior of invasive blue crab in Mediterranean microhabitats. Mediterr. Mar. Sci. 24, 229–240. https://doi.org/10.12681/mms.31332.
Martínez Prentice, R., Villoslada Peciña, M., Ward, R.D., Bergamo, T.F., Joyce, C.B., Sepp, K., 2021. Machine learning classification and accuracy assessment from high-resolution images of coastal wetlands. Remote Sens. 13, 3669. https://doi.org/10.3390/rs13183669.
Matiza, C., Mutanga, O., Odindi, J., Mngadi, M., 2024. The utility of Planetscope spectral data in quantifying above-ground carbon stock in an urban reforested landscape. Ecol. Inform. 80, 102472 https://doi.org/10.1016/j.ecoinf.2024.102472.
Melgani, F., Bruzzone, L., 2004. Classification of hyperspectral remote sensing images with support vector machines. IEEE Trans. Geosci. Remote Sens. 42, 1778–1790.
Mitsch, W.J., Bernal, B., Hernandez, M.E., 2015. Ecosystem services of wetlands. Int. J. Biodivers. Sci. Ecosyst. Serv. Manag. 11, 1–4. https://doi.org/10.1080/21513732.2015.1006250.
Miyamoto, E., Jr, T.M., 2008. Fast Calculation of Haralick Texture Features 6.
Molinaro, A.M., Simon, R., Pfeiffer, R.M., 2005. Prediction error estimation: a comparison of resampling methods. Bioinformatics 21, 3301–3307. https://doi.org/10.1093/bioinformatics/bti499.
Moritake, K., Cabezas, M., Nhung, T.T.C., Lopez Caceres, M.L., Diez, Y., 2024. Sub-alpine shrub classification using UAV images: performance of human observers vs DL classifiers. Ecol. Inform. 80, 102462 https://doi.org/10.1016/j.ecoinf.2024.102462.
Müllerová, J., Bartaloš, T., Brůna, J., Dvořák, P., Vítková, M., 2017. Unmanned aircraft in nature conservation: an example from plant invasions. Int. J. Remote Sens. 38, 2177–2198. https://doi.org/10.1080/01431161.2016.1275059.
Olsson, P-O, Vivekar, A, Adler, K, Garcia Millan, VE, Koc, A, Alamrani, M, Eklundh, L, 2021. Radiometric Correction of Multispectral UAS Images: Evaluating the Accuracy of the Parrot Sequoia Camera and Sunshine Sensor. Remote Sensing 13 (4), 577. https://doi.org/10.3390/rs13040577.
Persson, M., Lindberg, E., Reese, H., 2018. Tree species classification with multi-temporal Sentinel-2 data. Remote Sens. 10, 1794. https://doi.org/10.3390/rs10111794.
Peterson, A.T., Stewart, A., Mohamed, K.I., Araújo, M.B., 2008. Shifting global invasive potential of European plants with climate change. PLoS One 3, e2441. https://doi.org/10.1371/journal.pone.0002441.
Petrů, A., Pechar, L., Pecharová, E., 2016. The development of macro-scale vegetation in a fishpond ecosystem with considerably reduced fish stocking–a case study. In: International Multidisciplinary Scientific GeoConference: SGEM, pp. 693–700.
Phinzi, K., Abriha, D., Bertalan, L., Holb, I., Szabó, S., 2020. Machine learning for gully feature extraction based on a Pan-sharpened multispectral image: multiclass vs. binary approach. ISPRS Int. J. Geo Inf. 9, 252. https://doi.org/10.3390/ijgi9040252.
Phinzi, K., Holb, I., Szabó, S., 2021. Mapping permanent gullies in an agricultural area using satellite images: efficacy of machine learning algorithms. Agronomy 11, 333.
Pix4D SA, Switzerland, n.d..
R Core Team, 2023. R: A Language and Environment for Statistical Computing. R Foundation for Statistical Computing.
Rasel, S.M.M., Chang, H.-C., Ralph, T.J., Saintilan, N., Diti, I.J., 2021. Application of feature selection methods and machine learning algorithms for saltmarsh biomass

estimation using Worldview-2 imagery. Geocarto. Int. 36, 1075–1099. https://doi.org/10.1080/10106049.2019.1624988.
Recknagel, F., Staiano, A., 2019. Editorial: analysis and synthesis of ecological data by machine learning. Ecol. Inform. 53, 100971 https://doi.org/10.1016/j.ecoinf.2019.05.017.
Ribeiro-Souza, P., Graipel, M.E., Astúa, D., Vancine, M.H., Pires, J.S.R., 2022. Effects of climate change on distribution and areas that protect two neotropical marsupials associated with aquatic environments. Ecol. Inform. 68, 101570 https://doi.org/10.1016/j.ecoinf.2022.101570.
Richards, J.A., 2013. Remote Sensing Digital Image Analysis, 5th ed. Springer, Berlin.
Rotigliano, E., Martinello, C., Agnesi, V., Conoscenti, C., 2018. Evaluation of debris flow susceptibility in El Salvador (CA): a comparison between multivariate adaptive regression splines (MARS) and binary logistic regression (BLR). Hung. Geogr. Bull. 67, 361–373. https://doi.org/10.15201/hungeobull.67.4.5.
Rouse, J.W., Haas, R.H., Deering, D.W., Schell, J.A., Harlan, J.C., 1974. Monitoring the Vernal Advancement and Retrogradation (Green Wave Effect) of Natural Vegetation (No. E75-10354).
Sannigrahi, S., Chakraborti, S., Banerjee, A., Rahmat, S., Bhatt, S., Jha, S., Singh, L.K., Paul, S.K., Sen, S., 2020. Ecosystem service valuation of a natural reserve region for sustainable management of natural resources. Environ. Sustain. Indic. 5, 100014 https://doi.org/10.1016/j.indic.2019.100014.
Schlosser, A.D., Szabó, G., Bertalan, L., Varga, Z., Enyedi, P., Szabó, S., 2020. Building extraction using orthophotos and dense point cloud derived from visual band aerial imagery based on machine learning and segmentation. Remote Sens. 12, 2397. https://doi.org/10.3390/rs12152397.
Sen, R., Goswami, S., Chakraborty, B., 2019. Jeffries-Matusita distance as a tool for feature selection, in: 2019 international conference on data science and engineering (ICDSE). In: Presented at the 2019 International Conference on Data Science and Engineering (ICDSE), pp. 15–20. https://doi.org/10.1109/ICDSE47409.2019.8971800.
Szabó, L., Burai, P., Deák, B., Dyke, G.J., Szabó, S., 2019. Assessing the efficiency of multispectral satellite and airborne hyperspectral images for land cover mapping in an aquatic environment with emphasis on the water caltrop (Trapa natans). Int. J. Remote Sens. 40, 4876–4897. https://doi.org/10.1080/01431161.2019.1579383.
Szabó, L., Deák, B., Bíró, T., Dyke, G.J., Szabó, S., 2020. NDVI as a proxy for estimating sedimentation and vegetation spread in Artificial Lakes—monitoring of spatial and temporal changes by using satellite images overarching three decades. Remote Sens. 12, 1468.
Tan, W., Xing, J., Yang, S., Yu, G., Sun, P., Jiang, Y., 2020. Long term aquatic vegetation dynamics in Longgan Lake using Landsat time series and their responses to water level fluctuation. Water 12, 2178. https://doi.org/10.3390/w12082178.
Tucker, C.J., 1979. Red and photographic infrared linear combinations for monitoring vegetation. Remote Sens. Environ. 8, 127–150.
Tulldahl, H.M., Wikström, S.A., 2012. Classification of aquatic macrovegetation and substrates with airborne lidar. Remote Sens. Environ. 121, 347–357. https://doi.org/10.1016/j.rse.2012.02.004.
Tyler, T., Herbertsson, L., Olsson, P.A., Fröberg, L., Olsson, K., Svensson, Å., Olsson, O., 2018. Climate warming and land-use changes drive broad-scale floristic changes in southern Sweden. Glob. Chang. Biol. 24, 2607–2621. https://doi.org/10.1111/gcb.14031.
Varga, O.G., Kovács, Z., Bekő, L., Burai, P., Csatáriné Szabó, Z., Holb, I., Ninsawat, S., Szabó, S., 2021. Validation of visually interpreted corine land cover classes with spectral values of satellite images and machine learning. Remote Sens. 13, 857. https://doi.org/10.3390/rs13050857.
Walker, W.S., Stickler, C.M., Kellndorfer, J.M., Kirsch, K.M., Nepstad, D.C., 2010. Large-area classification and mapping of forest and land cover in the Brazilian Amazon: a comparative analysis of ALOS/PALSAR and landsat data sources. IEEE J. Sel. Top. Appl. Earth Obs. Remote Sens. 3, 594–604. https://doi.org/10.1109/JSTARS.2010.2076398.
Walter, A.C., 2020. Discrimination of Maize Genotypes through Multi-Temporal Object-Based Remote-Sensing Classification of Unmanned Aircraft System Images (Thesis).
Wang, Z., Liu, J., Li, J., Zhang, D.D., 2018. Multi-spectral water index (MuWI): a native 10-m multi-spectral water index for accurate water mapping on Sentinel-2. Remote Sens. 10, 1643. https://doi.org/10.3390/rs10101643.
Wang, X., Gao, X., Zhang, Yuanzhi, Fei, X., Chen, Z., Wang, J., Zhang, Yayi, Lu, X., Zhao, H., 2019. Land-cover classification of coastal wetlands using the RF algorithm for Worldview-2 and landsat 8 images. Remote Sens. 11, 1927. https://doi.org/10.3390/rs11161927.
Wilk-Woźniak, E., Walusiak, E., Burchardt, L., Cerbin, S., Chmura, D., Gąbka, M., Glińska-Lewczuk, K., Gołdyn, R., Grabowska, M., Karpowicz, M., Klimaszyk, P., Kołodziejczyk, A., Kokociński, M., Kraska, M., Król, W., Kuczyńska-Kippen, N., Ligęza, S., Messyasz, B., Nagengast, B., Ozimek, T., Paczuska, B.M., Pełechaty, M., Pęczuła, W., Pietryka, M., Piotrowicz, R., Pociecha, A., Pukacz, A., Richter, D., Żbikowski, J., 2019. Effects of the environs of waterbodies on aquatic plants in oxbow lakes (habitat 3150). Ecol. Indic. 98, 736–742. https://doi.org/10.1016/j.ecolind.2018.11.025.
Woellner, R., Wagner, T.C., 2019. Saving species, time and money: application of unmanned aerial vehicles (UAVs) for monitoring of an endangered alpine river specialist in a small nature reserve. Biol. Conserv. 233, 162–175. https://doi.org/10.1016/j.biocon.2019.02.037.
Xing, H., Niu, J., Feng, Y., Hou, D., Wang, Y., Wang, Z., 2023. A coastal wetlands mapping approach of Yellow River Delta with a hierarchical classification and optimal feature selection framework. CATENA 223, 106897. https://doi.org/10.1016/j.catena.2022.106897.